

Unusual Radio Properties of the BL Lac Object 0820+225

D. C. Gabuzda^{1,2}, A. B. Pushkarev² and N. N. Garnich³

¹*Joint Institute for VLBI in Europe, Postbus 2, 7990 AA Dwingeloo, The Netherlands*

²*Astro Space Centre, Lebedev Physical Institute, 53 Leninsky Pr., 117924 Moscow, Russia*

³*Sternberg Astronomical Institute, 13 Universitetskii pr., 119899 Moscow, Russia*

24 October 2018

ABSTRACT

We present the results of simultaneous VLBA polarisation observations of the BL Lacertae object 0820+225 at 5, 8, and 15 GHz, together with earlier images at 5 GHz. This source has an unusually rich total intensity and polarisation structure compared to other objects with comparable redshifts. The magnetic field in the inner part of the complex and highly twisted VLBI jet is transverse, as is typical of BL Lacertae objects, but becomes roughly longitudinal further from the core, possibly due to shear. Although the integrated rotation measure of 0820+225 is modest, the rotation-measure distribution on parsec scales is non-uniform, and clearly shows regions where the rotation measure is substantially higher than the integrated value.

Key words: magnetic fields – galaxies: quasars: individual: 0820+225

1 INTRODUCTION

BL Lacertae objects are highly variable, polarized, flat spectrum AGN that are distinguished from OVV quasars primarily by the absence of strong optical line emission. 5, 8.4, and 22 GHz global VLBI polarization observations have shown that the jet components in BL Lacertae objects are most often polarized with electric field parallel to the jet (Gabuzda, Pushkarev, & Cawthorne 2000; Gabuzda & Cawthorne 1996, 2000; and references therein). This has often been interpreted as evidence for transverse shocks that have compressed an initially random magnetic field \mathbf{B} , so that the net \mathbf{B} in the shocked region is perpendicular to the jet (Laing 1980; Hughes, Aller, and Aller 1989). Recently, evidence has been mounting that many of the transverse \mathbf{B} fields observed in the VLBI jets of these sources may instead be associated with the dominant toroidal component of a possibly helical jet \mathbf{B} field (Gabuzda 1999; Pushkarev & Gabuzda 2000; Gabuzda & Pushkarev 2001). We are undertaking a multi-frequency, multi-epoch VLBI study of the complete sample of BL Lacertae objects defined by Kühr & Schmidt (1990) in order to uncover the nature of the characteristic VLBI properties of these sources.

One of the advantages of making systematic observations of a complete sample is that we obtain information about a wide range of sources, not only a few of the brightest and, at first glance, most spectacular and interesting. This has proved to be very valuable in our multi-frequency (5, 8.4 and 15 GHz; February and April 1997) VLBA observations of sources in the Kühr & Schmidt sample. The object 0820+225 had not been studied previously using VLBI. This

source has proved itself to be a rather unusual member of this sample for a number of reasons. Its integrated 5-GHz flux is of the order of 1 Jy, but its VLBI structure is very extended, and the VLBI core contains only a small fraction of the total mas-scale flux. This is particularly remarkable because 0820+225 is one of only a half dozen of the sample sources with large redshifts, $z \sim 1$ or slightly greater. This combination of extremely extended structure at high redshift makes it unique among the sample sources. First-epoch 5 GHz images (Gabuzda, Pushkarev, & Cawthorne 2000) show that the VLBI jet is highly curved, and forms an overall “S-like” shape. The origin of this curvature is unclear; it is suggestive of some type of instability in or precession of the VLBI jet.

The two 5 GHz images presented here are second and third-epoch images. Overall, the 5 GHz VLBI structure of the source is relatively stable, showing a number of features that appear to be nearly stationary. The multi-frequency images presented here reveal the presence of substantial rotation-measure (RM) gradients both along and across the jet. After accounting for the parsec-scale RM distribution, the polarization vectors in the inner section of the jet are well aligned with the local jet direction, so that the magnetic field in this part of the jet is transverse. The polarization in the more extended part of the jet is somewhat offset toward the outer edge of the jet and implies a longitudinal field, suggesting a shear interaction with a surrounding medium. The observed rotation measures suggest that the thermal gas causing the Faraday rotation has properties that are fairly typical of narrow-line clouds.

2 OBSERVATIONS AND REDUCTION

2.1 5 GHz, epoch 1995.36

First-epoch global-VLBI I and P images of 0820+225 at 5 GHz have been presented by Gabuzda, Pushkarev, & Cawthorne (2000). Our second-epoch observations were obtained at epoch 1995.36 using a ten-station global array consisting of the Medicina (32 m), Effelsberg (100 m), St. Croix (25 m), Hancock (25 m), Green Bank (43 m), North Liberty (25 m), Owens Valley (25 m), Brewster (25 m), and Mauna Kea (25 m) antennas and the Westerbork phased array ($\sqrt{14} \times 25$ m). The observations were made under the auspices of the US and European VLBI networks. The north-south resolution provided by these observations is substantially improved due to the use of the two southern antennas St. Croix and Mauna Kea. The data were recorded using the MkIII system, and the data were subsequently correlated using the Mk IIIA correlator at the Max-Planck-Institut-für-Radioastronomie in Bonn.

The data reduction and imaging were done in the Brandeis VLBI package. The polarization calibration of these data was performed as described by Roberts, Wardle and Brown (1994). The instrumental polarizations for each antenna were determined from observations of the unpolarized sources 3C84 and OQ208. The absolute orientation of the polarization position angles was calibrated using VLBI observations of several compact polarized sources together with measurements of their integrated polarizations derived from nearly simultaneous VLA observations. The final uncertainty in the polarization position angles is about $2 - 3^\circ$.

Images of the distribution of total intensity I were made using a self-calibration algorithm similar to that described by Cornwell and Wilkinson (1981). Maps of the linear polarization^{*} P were made by referencing the calibrated cross-hand fringes to the parallel-hand fringes using the antenna gains determined in the hybrid mapping, Fourier transforming the cross-hand fringes, and performing a complex CLEAN. This procedure registers the I and P maps to within a small fraction of a beamwidth.

2.2 Multi-frequency, epoch 1997.11

Our multi-frequency observations of 0820+225 were made in February 1997 (1997.11) with the ten antennas of the NRAO Very Long Baseline Array[†]. Observations were obtained simultaneously at 15, 8.4, and 5 GHz with full polarization sensitivity. The data were calibrated and imaged in the NRAO AIPS package using standard techniques.

The strong source 3C84, which is essentially unpolarized at these wavelengths, was used to determine the instrumental polarizations of each antenna at each frequency. The absolute orientation of the polarization position angles was calibrated using VLBA observations of the compact,

^{*} $P = pe^{2i\chi} = mIe^{2i\chi}$, where $p = mI$ is the polarized intensity, m is the fractional linear polarization, and χ is the position angle of the electric vector on the sky, measured from north through east.

[†] The National Radio Astronomy Observatory (NRAO) is a facility of the National Science Foundation operated under cooperative agreement by Associated Universities, Inc.

strongly polarised source 1823+568 together with measurements of its integrated polarization from VLA data obtained roughly one day after the end of the VLBA run. Here, also, the resulting uncertainty in the absolute χ values is about $2 - 3^\circ$ at all frequencies.

3 RESULTS AND DISCUSSION

Figures 1–4 show contour images of the total or linearly polarized flux density, with superposed sticks showing the orientation of the polarization position angles χ . In each of the images, the restoring beam is indicated by a cross or ellipse in some corner of the map. Note that the I and P beams for the 1995.36 images in Fig. 1 are rather different; we show the P image restored with its own beam in order to accurately reflect the different baseline coverages for the I and P datasets.

3.1 Total Intensity Structure

The VLBI structure of 0820+225 is very rich in both I and P . Our 5 GHz images, shown in Figs. 1 and 2, follow the VLBI jet roughly 30 mas from the core. For ease of comparison, the contour levels in mJy for the I images in Fig. 1 and the highest 12 contour levels in mJy for the I images in Fig. 2 coincide. We can see that, in contrast to the overwhelming majority of BL Lacertae objects, the bulk of the parsec-scale flux is contained in the jet rather than the core. The VLBI jet bends quite strongly, in a shape that is suggestive of some type of precession or oscillatory instability. The 8.4 GHz image in Fig. 3a shows the extended VLBI jet in somewhat more detail. The jet gives the impression of being continuous, but also shows clear clumpiness in the brightness distribution. The 15 GHz image in Fig. 4a shows the inner part of the curved VLBI jet with higher resolution. The knotty structure of the jet is clearly visible.

Figure 5 shows the distribution of the spectral index calculated between 5 and 8.4 GHz, α_{5-8} ($S \propto \nu^\alpha$). We can see that all regions of the VLBI structure have steep spectra, indicating that they are optically thin. The spectral index throughout most of the outer jet is $\alpha_{5-8} \simeq -2.0$ to -2.5 , while the spectra are less steep near the core and in the inner jet ($\alpha_{5-8} \simeq 0$ to -1). The spectrum is actually flattest near the westward bend, near the position of C2 (see Fig. 6).

3.2 Rotation Measure Distribution on Parsec Scales

Only two polarized features are detected in the inner part of the jet, and these are detected at all three frequencies. A comparison of the inner-jet region in the polarization images in Figs. 2b, 3b, and 4b immediately demonstrates the presence of a non-uniform frequency dependence for the observed polarization position angles. The knot roughly 3 mas from the core (“C1”) has nearly the same χ values at all three frequencies; in contrast, the three χ values for the knot roughly 6 mas from the core (“C2”) are very different. The top plot in Fig. 6 clearly shows that the observed χ values for both knots are consistent with λ^2 dependences ($\lambda = c/\nu$

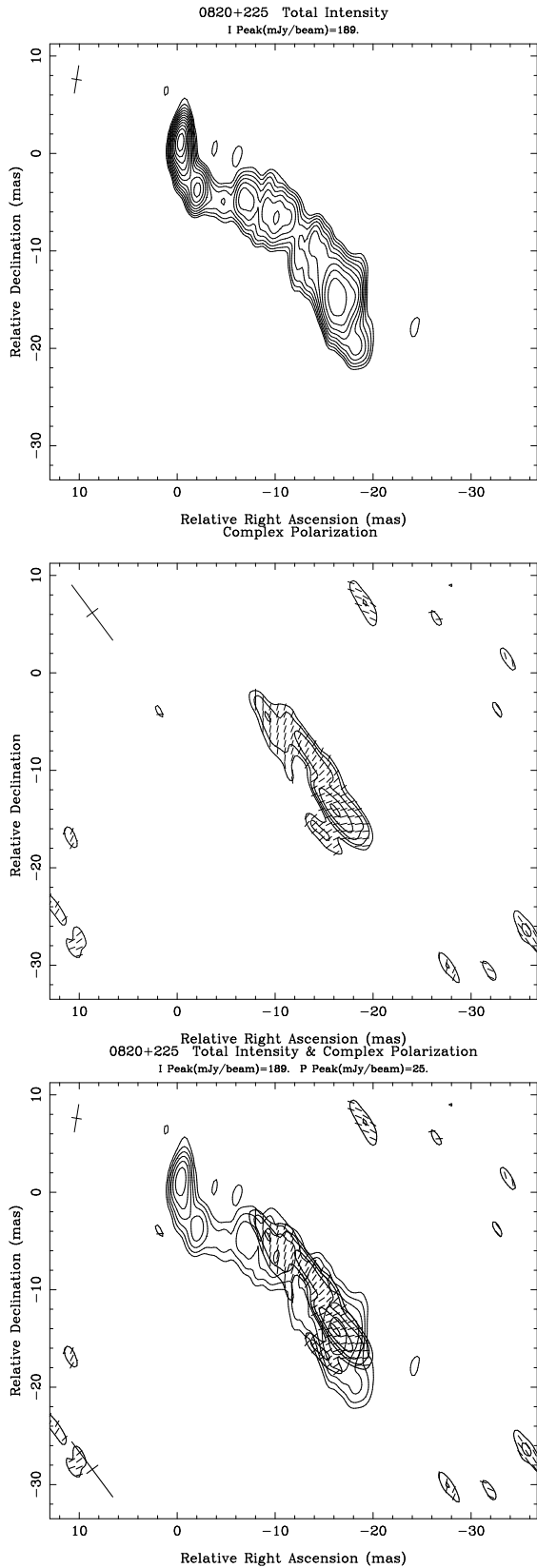


Figure 1. VLBI images of 0820+225 at 5 GHz at epoch 1995.36: (a) I with contours at $-1.8, 1.8, 2.6, 3.6, 5.1, 7.2, 10, 14, 20, 29, 41, 58,$ and 82% of the peak brightness of 188.7 mJy/beam. (b) p with contours at $24, 34, 45, 64,$ and 90% of the peak brightness of 25 mJy/beam and χ sticks superimposed. (c) The I image from (a) with every other contour omitted and χ sticks superimposed. Note that the I and P beams are quite different in this case.

© 0000 RAS, MNRAS 000, 000–000

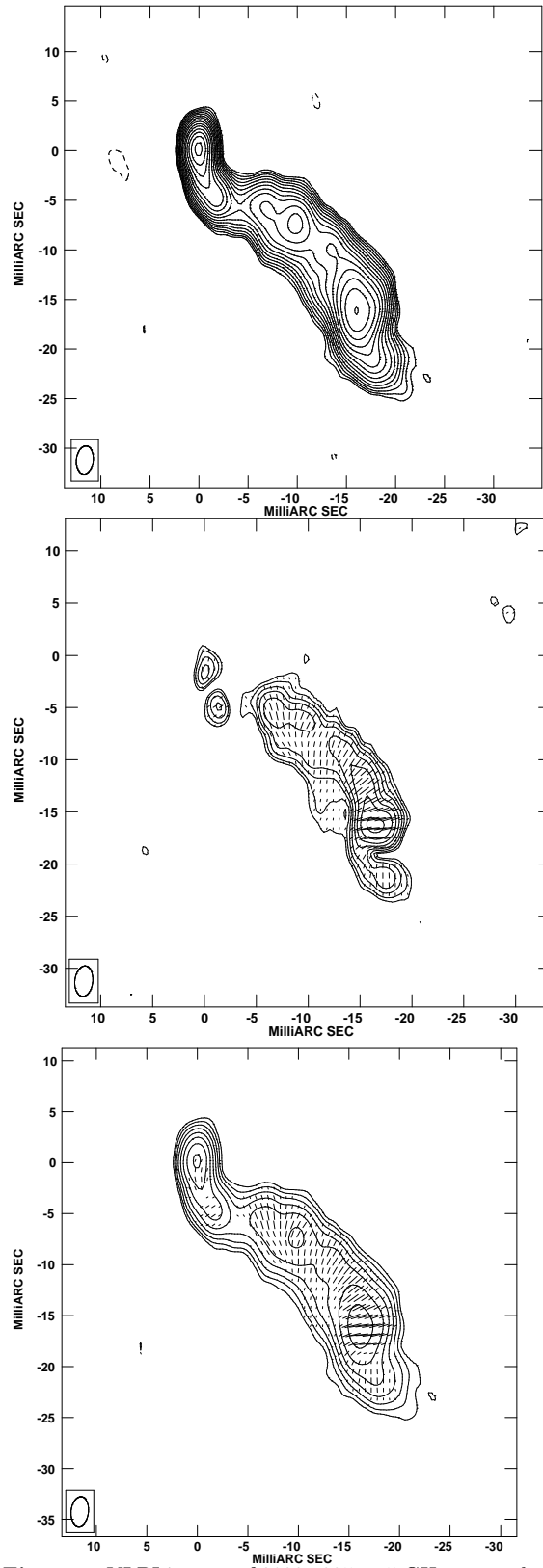


Figure 2. VLBI images of 0820+225 at 5 GHz at epoch 1997.11: (a) I with contours at $-0.7, 0.7, 1.0, 1.4, 2.0, 2.8, 4.0, 5.6, 8.0, 11, 16, 23, 32, 45, 64,$ and 90% of the peak brightness of 167.1 mJy/beam. (b) p with contours at $8, 11, 16, 23, 32, 45, 64,$ and 90% of the peak brightness of 13.2 mJy/beam and χ sticks superimposed. (c) The I image from (a) with every other contour omitted and χ sticks superimposed.

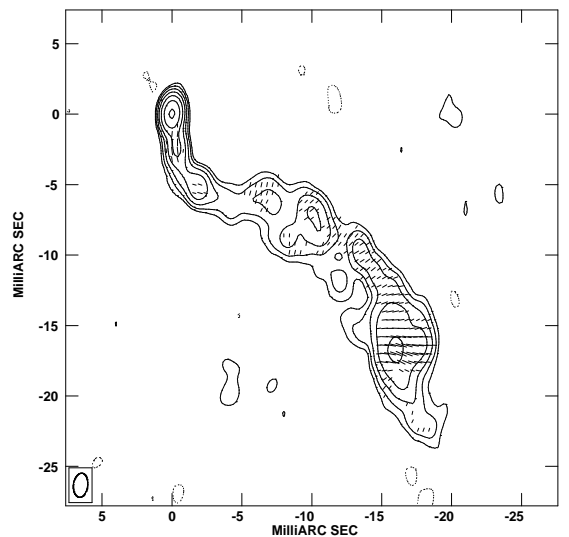
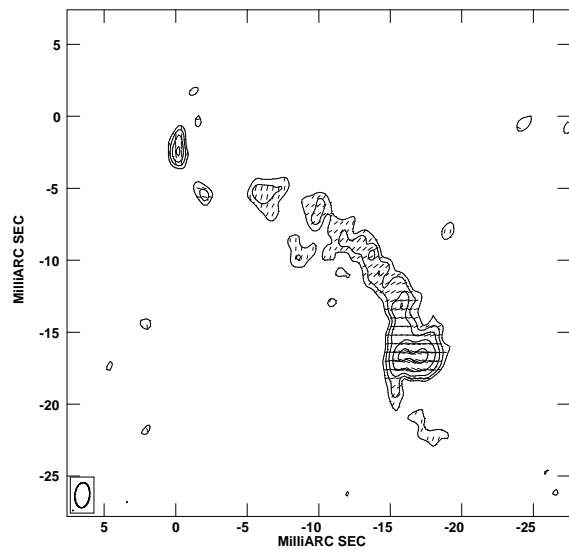
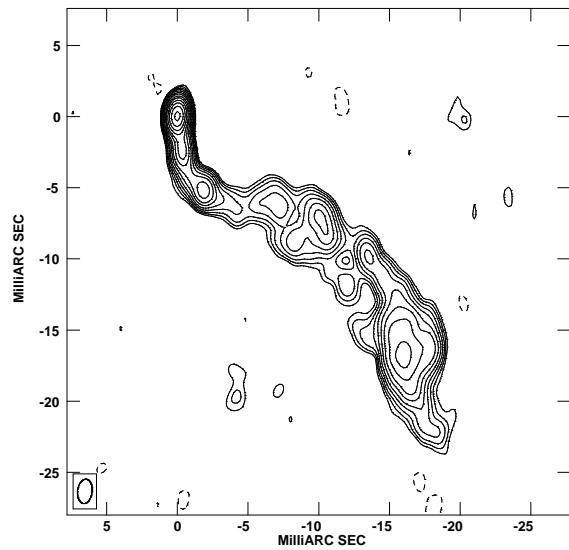


Figure 3. VLBI images of 0820+225 at 8.4 GHz at epoch 1997.11: (a) I with contours at $-1.4, 1.4, 2.0, 2.8, 4.0, 5.6, 8.0, 11, 16, 23, 32, 45, 64,$ and 90% of the peak brightness of 112.2 mJy/beam. (b) p with contours at $23, 32, 45, 64,$ and 90% of the peak brightness of 4.5 mJy/beam and χ sticks superimposed. (c) The I image from (a) with every other contour omitted and χ sticks superimposed.

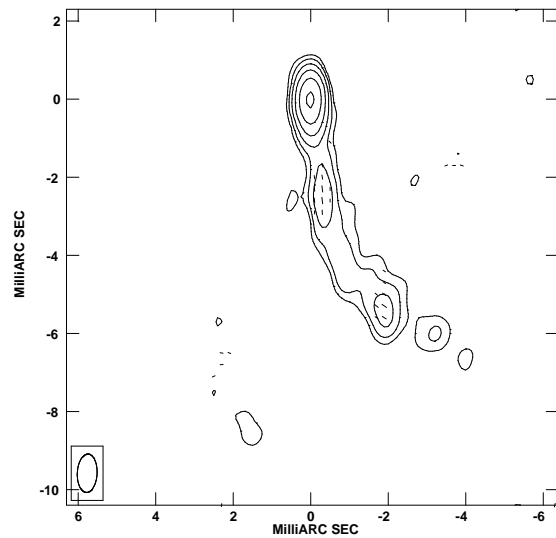
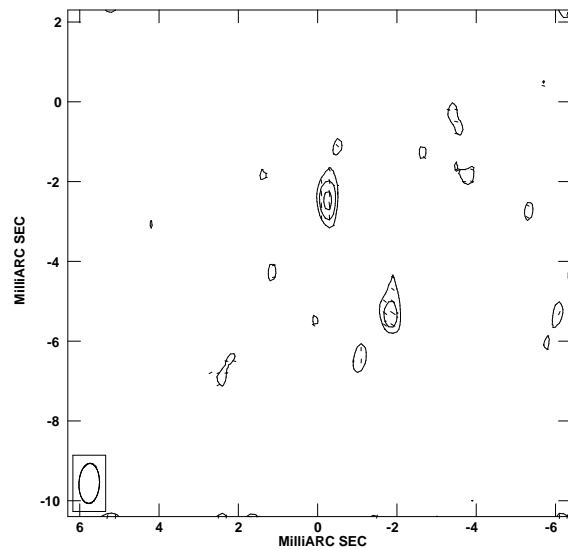
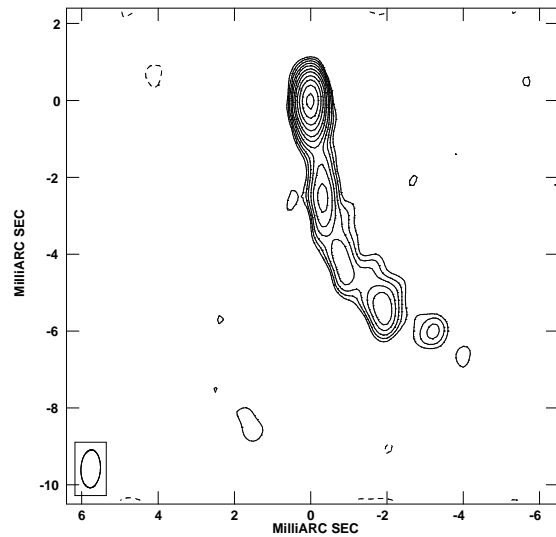


Figure 4. VLBI images of 0820+225 at 15 GHz at epoch 1997.11: (a) I with contours at $-2.8, 2.8, 4.0, 5.6, 8.0, 11, 16, 23, 32, 45, 64,$ and 90% of the peak brightness of 109.0 mJy/beam. (b) p with contours at $45, 64,$ and 90% of the peak brightness of 3.4 mJy/beam and χ sticks superimposed. (c) The I image from (a) with every other contour omitted and χ sticks superimposed.

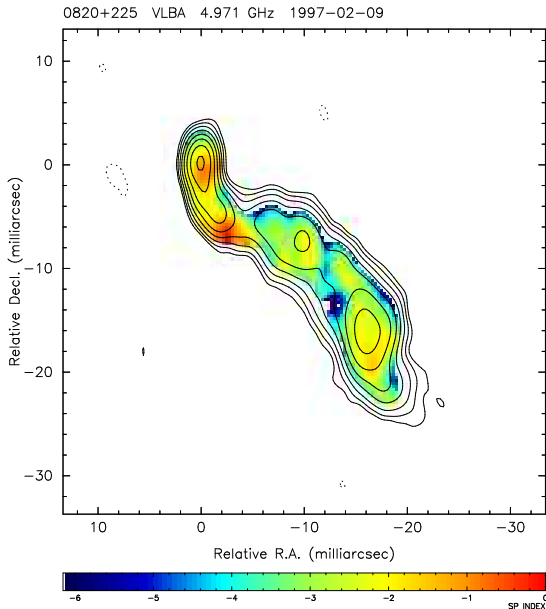


Figure 5. I images of 0820+225 at 5 GHz at epoch 1997.11 from Fig. 2c with the distribution of the spectral index calculated between 5 and 8.4 GHz superimposed.

is the observing wavelength), as expected for Faraday rotation: the inferred rotation measure for the inner knot is only $+42 \text{ rad/m}^2$, while that for the outer knot is $+353 \text{ rad/m}^2$.

Polarized flux further from the core is detected only at 5 and 8.4 GHz. Therefore, we cannot strictly test there for a λ^2 dependence of the measured χ values. Nonetheless, we can compare the χ 's observed at the two frequencies and calculate the rotation measure implied if any difference is, indeed, due to external Faraday rotation. Figure 6 (bottom) shows the distribution of the inferred RMs based on a comparison of the images for the two lower frequencies; in the inner jet, these RMs are consistent with those derived using all three frequencies. There is evidence for inhomogeneity in the RM distribution in the outer jet as well; there is another region of high RM just to the west of the dip in the jet intensity about 8 mas from the core.

In general, the observed RMs decrease with distance from the core in the outer part of the jet. The RMs in the outer jet remain somewhat inhomogeneous, but have more modest values, some roughly comparable to the integrated RM determined using 1.50 and 1.67 GHz VLA observations, $+81 \text{ rad/m}^2$ (Pushkarev 2001). Since the 8.4 and 5 GHz polarization images presented here are already dominated by the outer jet, and this trend should continue toward lower frequencies, we expect that the 1.50–1.67 GHz polarization will be dominated by the contribution of regions lying $\simeq 15 \text{ mas}$ or more from the core. The fact that the RMs inferred here for some parts of the outer jet are roughly comparable to the integrated value may indicate that we are just starting to detect a constant “foreground,” presumably

Galactic, rotation measure. However, a substantial fraction of the outer 5-GHz jet has RMs that appreciably exceed the nominal integrated value, so that there is probably some contribution to the observed RMs from thermal plasma in the immediate vicinity of the BL Lac object throughout most of the observed 5-GHz VLBI jet. There is also some evidence that the observed RMs tend to be higher toward the southern edge of the jet; the physical origin for such a gradient is not clear.

Comparing Figs. 5 and 6 (bottom), we can see that the 5–8.4 GHz spectrum flattens in the core (as is expected) and also near the westward bend in the jet, where the rotation measures are highest. This is suggestive of either low-frequency absorption near this bend, or possibly of re-acceleration of electrons at this location. Both would be consistent with an interaction between the jet and external medium, and it is possible that this is related to the bending of the jet itself. We cannot test this idea more fully, however, since we were not able to image the region near and beyond this bend at 15 GHz, where we would expect absorption to be appreciably lower than at 5 GHz.

3.3 Linear Polarisation Structure After “De-rotation”

Thus, the rotation-measure distribution is quite non-uniform, and the Faraday rotations implied in the regions of highest rotation measure at the lowest observed frequency can reach $\sim 60 - 70^\circ$. Therefore, it is essential to correct for the observed rotation measure distribution if we wish to infer the intrinsic values for χ , and thereby the underlying magnetic field structure. Figure 7 shows the result of this correction. Here, we have adjusted the observed χ values in accordance with the rotation-measure distribution in Fig. 6 (bottom), then rotated the result by 90° so that it shows the distribution of the underlying magnetic field implied by the “de-rotated” χ values. Recall that all the observed 5 GHz components, including the core, are dominated by optically thin emission (Fig. 5), so that \mathbf{B} is perpendicular to the polarization electric vector.

This figure shows that the magnetic field in the inner part of the jet, before the westward bend, is transverse to the local jet direction, and that the dominant field becomes longitudinal beyond this bend. In addition, inspection of Figs. 3b and 2b shows that the polarized emission in the outer part of the VLBI jet is offset toward the northern edge of the main ridge lines in the corresponding I images. These properties are suggestive of an interaction between the jet and surrounding medium that enhances the longitudinal field component due to shear. The dominant magnetic field is longitudinal essentially throughout the outer portion of the jet. The inferred magnetic field pattern in the bright component roughly 20 mas from the core is complex. If the magnetic field sticks in this component in Fig. 7 reflect the direction of the underlying jet flow, this indicates that the jet turns sharply southward, then back eastward before continuing westward at the end of the visible jet; this is plausible, but must be verified by analysis of component motions in this region.

Figure 8 shows distributions of the degree of polarization m superposed on I images at 8.4 and 5 GHz. In each case, we include only those m values for pixels where both

0820+225

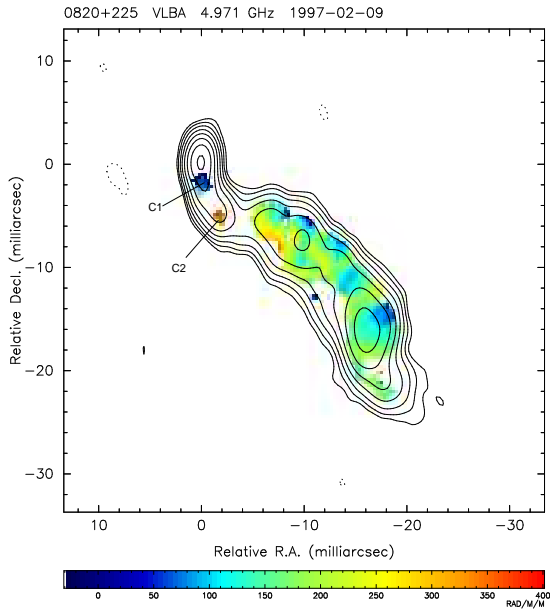
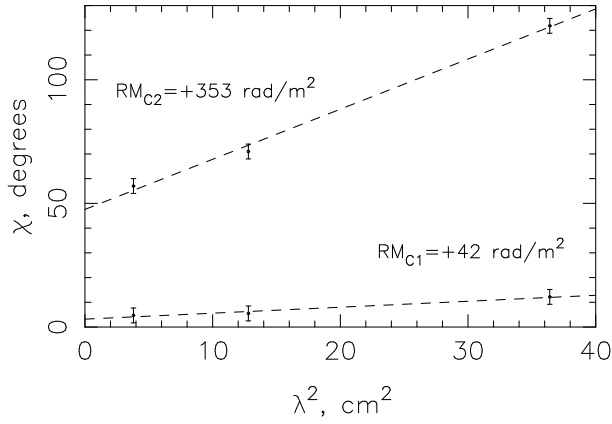


Figure 6. Top: Polarization position angles χ as a function of the square of the wavelength λ^2 for the two inner knots in the VLBI jet of 0820+225. The wavelength dependence of both components is consistent with a λ^2 law, but the rotation measure of the second knot, “C2,” is clearly much higher than that of the knot closest to the core, “C1.” Bottom: I image of 0820+225 at 5 GHz from Fig. 2c with the rotation-measure distribution calculated from the 5 and 8.4-GHz polarization maps superimposed.

polarization and total-intensity were clearly detected. We can see that m in the jet is typically $\simeq 10 - 15\%$, and reaches 30–40% or more in some places. In the 5 GHz m distribution, the degree of polarization increases toward the outer edge of the curved jet structure, consistent with the possibility that the longitudinal field has been more highly ordered there, where the shear interaction is strongest. The most unusual feature in the m distribution at 8.4 GHz is

the rather high inferred polarization in a region of low total intensity about 13 mas west and 8 mas south of the core. The map in Fig. 3b clearly shows the detection of polarized flux in this location, and gives no indication of a dip in polarized flux in the location of the dip in total intensity. If this region of high polarization – indicating a region of very highly ordered longitudinal field – is real, its origin is not obvious. One possibility is that the regions occupied by various components in the extended part of the jet have a much stronger transverse field component than this low-intensity region, which partially cancels the longitudinal field due to shear.

3.4 Estimation of the Magnetic-Field Strength and Properties of the Thermal Gas

Let us suppose that the thermal gas giving rise to the large RM in the vicinity of the westward bend just beyond “C2” has properties fairly typical of a narrow-line cloud. In particular, we will assume that its temperature is $T \simeq 10^4$ K, as has been established from observations of forbidden and semi-forbidden lines (Koski 1978; Heckman & Balick 1979). If we then assume further that this cloud is in equipartition, we can derive at least a rough estimate for the magnetic field in this region using the relations (Burn 1966; Tucker 1975)

$$RM = 8.1 \times 10^5 \int N_e \vec{B} \cdot d\vec{l}$$

$$RM \simeq 8.1 \times 10^5 N_e B_{\parallel} L$$

$$N_e kT \simeq \frac{B^2}{8\pi}$$

where the first equation gives the definition of the rotation measure and the second is an approximation to the RM for the case of electromagnetic radiation travelling a length L through a region of homogeneous thermal plasma with the magnetic-field component along the line of sight equal to B_{\parallel} . Here, L is in pc, B and B_{\parallel} are in G, the electron number density N_e is in cm^{-3} , and RM is in rad m^{-2} . Eliminating N_e and multiplying the observed rotation measure by $(1+z)^2$ to determine the RM in the source frame, we obtain

$$B^2 B_{\parallel} \simeq \frac{RM(1+z)^2 \pi kT}{10^5 L}$$

Approximating $B_{\parallel} \simeq B$, as we expect if the magnetic field has no special orientation relative to the line of sight to the radio source (this approximation should affect the final result by at most about a factor of two or so),

$$B^3 \simeq \frac{RM(1+z)^2 \pi kT}{10^5 L}$$

$$B \simeq \left[\frac{RM(1+z)^2 \pi kT}{10^5 L} \right]^{1/3}$$

$$B \simeq 3.8 \times 10^{-5} L^{-1/3}.$$

Further, we have some idea of the size of the region of thermal gas giving rise to the rotation measure, based on the extent of the region of high rotation measure on the sky –

say, about 5 mas. If the thermal-gas cloud were much bigger than this, we would expect the observed region of high rotation measure to be larger. Since $1 \text{ mas} = 5.64 \text{ pc}$ at the redshift of 0820+225 ($H_0 = 75 \text{ km s}^{-1} \text{ Mpc}^{-1}$, $q_0 = 0.5$), this implies a diameter L of about 20–30 pc, which is reasonable, given estimates of the size of the narrow-line region for nearby AGNs ($r \simeq 100 \text{ pc}$ or slightly larger; Peterson 1997). Substituting this value into our expression for B , we obtain the estimate $B \simeq 12 - 14 \mu\text{G}$ for this region several tens of parsecs from the VLBI core, consistent with general expectations for the strength of the magnetic field on parsec scales (perhaps $10 - 100 \mu\text{G}$) and the inferred magnetic field on kiloparsec scales ($\simeq 0.15 - 1.5 \mu\text{G}$; see for example, Laing & Bridle 1987). While it does not provide us with precise estimates, this analysis does suggest parameters for the thermal gas associated with the Faraday rotation and the region in which it is located that are consistent with current concepts about narrow-line clouds.

4 CONCLUSION

Based on our earlier 5 GHz I and P VLBI images of 0820+225 (Gabuzda, Pushkarev & Cawthorne 2000), we already knew that this was an unusual source. It made it into the Kühr & Schmidt (1990) 1-Jy sample of BL Lac objects because its integrated flux at 5 GHz is, indeed, more than 1 Jy. Like the other sample sources, a high fraction of its integrated flux is on milliarcsecond scales. However, in sharp contrast to the other sources in the sample, only a small fraction of the flux on VLBI scales is contained in the VLBI core. The jet is very extended, especially given that the redshift of the source is relatively large for a BL Lac object, $z = 0.95$; this means that the VLBI jet sprawls over some 150–200 pc, with much of the emission located at substantial distances from the VLBI core.

The multi-frequency VLBA images presented here have underlined the unusual nature of this object by revealing an extremely non-uniform distribution for the rotation-measure on milliarcsecond scales. Galactic clouds of thermal plasma would be far too large to account for inhomogeneity in the rotation measure on such small angular scales. It is virtually certain that the thermal plasma giving rise to the non-uniform Faraday rotation is in the immediate environment of the VLBI jet. Therefore, since the RM is larger by a factor of $(1+z)^2$ in the rest frame of the source, the intrinsic RM of the component “C2” 6 mas from the core is about 1300 rad m^{-2} , and the RM gradient in this part of the jet is $\simeq 400 \text{ rad m}^{-2} \text{ mas}^{-1}$.

In addition, we have found compelling evidence for the formation of a shear layer in the outer part of the VLBI jet of 0820+225. While the inferred magnetic field in the inner part of the jet (after correction for the measured RM distribution) is transverse, the predominant magnetic field in the outer jet becomes longitudinal. The ordering of the longitudinal field in the outer jet is substantial, as indicated by the observed degrees of polarization at both 5 and 8.4 GHz, which reach $\simeq 30 - 40\%$. The degree of polarization across the 5-GHz jet increases toward the outer edge, consistent with the idea that it is here that the enhancement of the longitudinal field component by the shear interaction is strongest, as might be expected.

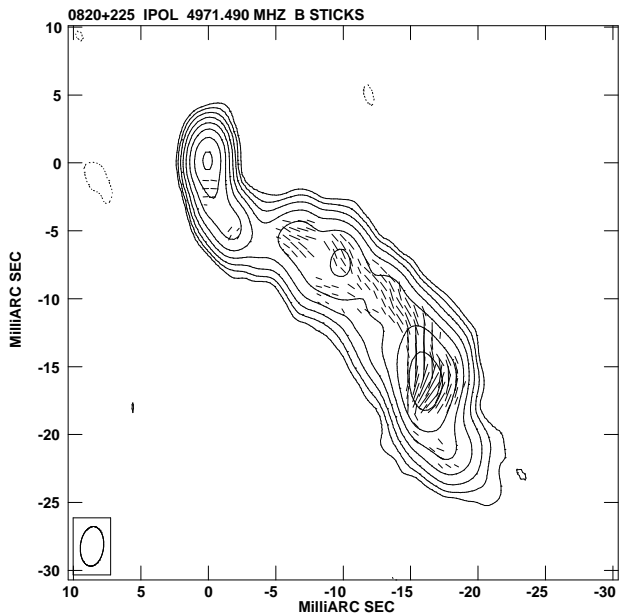


Figure 7. I image of 0820+225 at 5 GHz from Fig. 2c with the inferred intrinsic underlying \mathbf{B} field superimposed.

Thus, 0820+225 provides us with an interesting, seemingly paradoxical, combination of properties: very weak optical line emission, but clear evidence for the presence of appreciable quantities of thermal gas in the immediate vicinity of the AGN. This suggests that the weak line emission in this object is not simply due to a lack of gas: the gas is present, but is either not exposed to ionizing continuum radiation or is in a hot phase not conducive to the formation of dense clouds (Corbett et al. 1996).

Given the recent detection of a non-uniform parsec-scale RM distribution in BL Lac itself as well (Reynolds et al. 2001), this presents the interesting possibility that the weak optical line emission characteristic of these sources is generally not associated with a dearth of thermal gas. Since there is no clear evidence that BL Lac objects are more beamed than core-dominated quasars (Ghisellini et al. 1993), it is also implausible that the optical continua of BL Lac objects as a class are so much more highly beamed than the continua of quasars that their emission lines are “swamped,” giving rise to a featureless continuum. Thus, the most simple and plausible explanation for the weakness of the optical emission lines of BL Lac objects may be that the ionizing continuum radiation is insufficient to produce optical lines as luminous as those in quasars. In the framework of unification schemes identifying the FR I radio galaxies as the parent population of BL Lac objects (Browne 1983; Wardle, Moore & Angel 1984), this is also consistent with the analysis of Baum et al. (1995), who found the optical emission lines of FR I radio galaxies to be systematically less luminous than those of FR II radio galaxies of the same total radio luminosity or radio core power, and concluded that this was most likely associated with a lack of ionizing uv

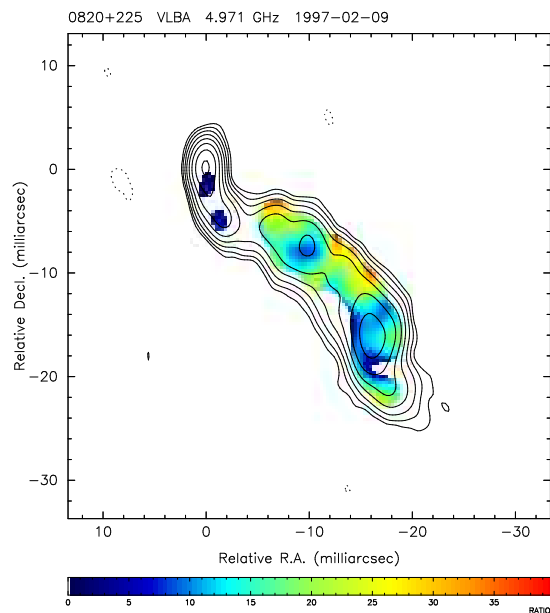
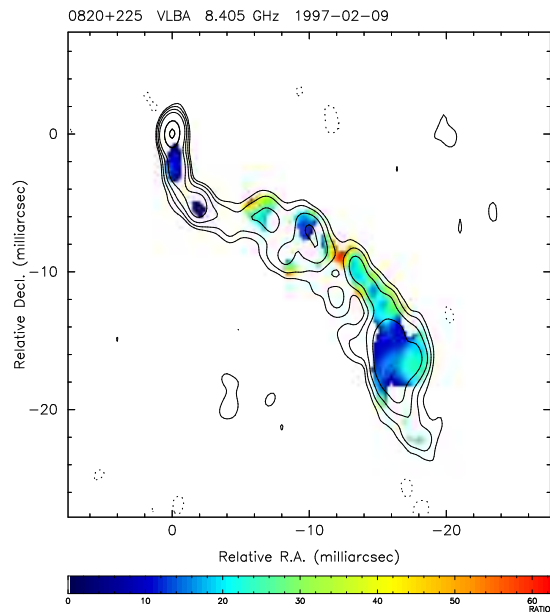


Figure 8. 8.4 and 5 GHz I images from (top) Fig. 3b and (bottom) Fig. 2b with the corresponding distributions of degree of polarization m displayed in grey scale superimposed.

continuum in FR I sources, rather than a lack of thermal gas.

We are currently engaged in a multi-epoch, multi-frequency VLBA project to study this object in more detail, and to search for possible superluminal motions and variations in the RM distribution. Such variations do not require changes in the Faraday screen (movement of blobs of thermal plasma, for example); the observed RM distribution could vary due to changes in the distribution of polarized emission behind the non-uniform Faraday screen. In this way, we hope that our multi-epoch study will provide further valuable information about both the distribution of thermal plasma in the vicinity of the BL Lac object and the properties of the unusual VLBI jet itself.

5 ACKNOWLEDGEMENTS

ABP acknowledges support from the Russian Foundation for Basic Research (project code 99-0217799). DCG acknowledges support from the European Commission under the IHP Programme (ARI) contract No. HPRI-CT-1999-00045. We thank L. Gurvits for useful discussions in connection with this work.

REFERENCES

- Baum S. A., Zirbel E. L., & O’Dea C. P., 1995, *ApJ*, 451, 88
 Browne I. W. A., 1983, *MNRAS*, 204, 23P
 Burn B. J., 1966, *MNRAS*, 133, 67
 Corbett E., Robinson A., Axon D., Hough J., Jeffries R., Thurston M., Young S., 1996, *MNRAS*, 281, 737
 Cornwell T. J., Wilkinson P. N., 1981, *MNRAS*, 196, 1067
 Gabuzda D. C., 1999, *New Astronomy Reviews*, 43, 691
 Gabuzda D. C. & Cawthorne T. V., 2000, *MNRAS*, 319, 1056
 Gabuzda D. C. & Cawthorne T. V., 1996, *MNRAS*, 283, 759
 Gabuzda D. C. & Pushkarev A. B., 2001, *Particles and Fields in Radio Galaxies*, Ed. R. Laing & K. Blundell, in press
 Gabuzda D. C., Pushkarev A. B., & Cawthorne T. V. 2000, *MNRAS*, 319, 1109
 Ghisellini G., Padovani P., Celotti A., & Maraschi L., 1993, *ApJ*, 407, 65
 Heckman T. M. & Balick B., 1979, *A&A*, 79, 350
 Hughes P. A., Aller H. D., & Aller M. F., 1989, *ApJ*, 341, 68
 Koski A. T., 1978, *ApJ*, 223, 56
 Kühn H. & Schmidt G., 1990, *AJ*, 90, 1
 Laing R., 1980, *MNRAS*, 193, 439
 Laing R. A. & Bridle A. H., 1987, *MNRAS*, 228, 557
 Peterson B. M., 1997, *An Introduction to Active Galactic Nuclei*, Cambridge: Cambridge University Press, p. 101–102
 Pushkarev A. B., 2001, *Astron. Rep.*, in press.
 Pushkarev A. B. & Gabuzda D. C., 2000, *Proceedings of the 5th EVN Symposium*, Eds. J. Conway, A. Polatidis, & R. Booth, Gothenburg (Sweden): Onsala Space Observatory
 Reynolds C., Cawthorne T. V., & Gabuzda D. C., 2001, *MNRAS*, submitted
 Roberts D.H., Wardle J.F.C., Brown L.F., 1994, *ApJ*, 427, 718
 Tucker W. H., 1975, *Radiation Processes in Astrophysics*, Cambridge, MA: Massachusetts Institute of Technology, p. 50
 Wardle J. F. C., Moore R. L., & Angel, J. R. P., 1984, *ApJ*, 279, 93